

Sgluon Pair Production to Next-to-Leading Order

Dorival Gonçalves Netto,¹ David López-Val,¹ Kentarou Mawatari,² Tilman Plehn,¹ and Ioan Wigmore³

¹*Institut für Theoretische Physik, Universität Heidelberg, Germany*

²*Theoretische Natuurkunde and IIHE/ELEM, Vrije Universiteit Brussel, Belgium
and International Solvay Institutes, Brussels, Belgium*

³*SUPA, School of Physics & Astronomy, The University of Edinburgh, UK*

Scalar color octets are generic signals for new physics at LHC energies. We examine their pair production at the LHC to next-to-leading order QCD. This computation serves as another test of the fully automatized MadGolem framework. We find large NLO production rates and sizeable quantum effects which depend on the sgluon mass. The shift in the sgluon distributions is mild and in good agreement with a multi-jet merging calculation.

I. INTRODUCTION

Sgluons [1, 2] are a type of scalar color octet states which arises in a variety of extensions of the Standard Model [3]. They can be fundamental or composite degrees of freedom. In extended supersymmetric models like the R -symmetric MSSM [1, 4, 5] or $\mathcal{N} = 1/\mathcal{N} = 2$ hybrid models [2], sgluons emerge as scalar partners of a Dirac gluino. More generally, sgluons appear to be ubiquitous in models of supersymmetry breaking [6]. Compositeness models include fermion fields which transform under a confining gauge group — some of them as fundamentals and others as anti-fundamentals. This naturally leads to scalar states in the $3 \otimes \bar{3} = 1 \otimes 8$ color-adjoint representations. This mechanism is realized in technicolor and top-color, chiral-color, and vector-like confinement [7]. In the presence of extra dimensions, color octet scalars emerge as low-lying Kaluza-Klein modes of the bulk gluon field [8].

At the LHC sgluon pairs will be copiously produced just through their couplings to gluons. In addition, for large masses, the model dependent single sgluon production channel might be competitive [1, 2, 9]. Available studies include the single and pairwise production in the context of supersymmetric scenarios [1, 2, 10], GUTs [11], extra dimensions [8, 12], as well as more model-independent approaches [13, 14]. Color-octet vector bosons have also been considered [15]. Distinctive decay patterns appear through couplings to pairs of SM particles or new heavy colored states. The most generic signature is the decay to two quark or gluon jets, $pp \rightarrow GG^* \rightarrow 4$ jets, possibly including bottom jets [16]. Subjet techniques [17] or suitable cuts on jet pair invariant masses [18, 19] have been proposed to handle the overwhelming QCD background. In supersymmetric models with Dirac gluinos the constraints on squark mixing are so weak that an essentially unconstrained squark mass matrix will lead to sgluon decays to single top (anti-) quarks plus a light jet, $G \rightarrow t\bar{q}, \bar{t}q$ [1]. Finally, highly isotropic multi-jet signatures $pp \rightarrow GG^* \rightarrow t\bar{t}\bar{t} \rightarrow 8j + 2\ell + \cancel{E}_T$ are likely for sufficiently heavy sgluons [1, 18]. Complementary rare decays [20] or long-lived bound states [21] are other potential discovery modes for novel color-adjoint scalars.

In this paper we present a complete next-to-leading order QCD calculation of sgluon pair production at the LHC. We examine the features and quantitative impact of the QCD quantum effects on the production rates and sgluon distributions. Our results are implemented in the MADGRAPH framework through the dedicated MADGOLEM package for the production of new particles to next-to-leading order [22]. This tool automatically computes next-to-leading order QCD corrections for any heavy particle production process and will be publicly available after the current testing phase. The NLO sgluon distributions we compare to the matched [23, 24] results for the combined process $pp \rightarrow GG^* + \text{jets}$.

Using the renormalizable supersymmetric realization the gluonic QCD corrections to sgluon pair production are obviously well defined. Additional supersymmetric QCD corrections are suppressed by the squark and gluino masses and thus negligible [25, 26]. Because we are only interested in sgluon pair production we can decouple all supersymmetric partners except for the sgluon, retaining all benefits of a renormalizable theory. This theory can as well be interpreted as the relevant QCD part of an effective strongly interacting theory.

II. SGLUON PAIR PRODUCTION TO NLO

To compute the complete NLO corrections for sgluon pair production at the LHC we minimally extend the Standard Model by one additional color octet, weak singlet, electrically neutral, and complex scalar field G . The sgluon couples to the Standard Model through the covariant derivative, $D_\mu G^A \equiv \partial_\mu G^A + g_s f^{ABC} G^B A_\mu^C$, where A_μ^C denotes the gluon field, g_s the strong coupling constant, and f^{ABC} the adjoint $SU(3)$ generators. The Feynman diagrams for the

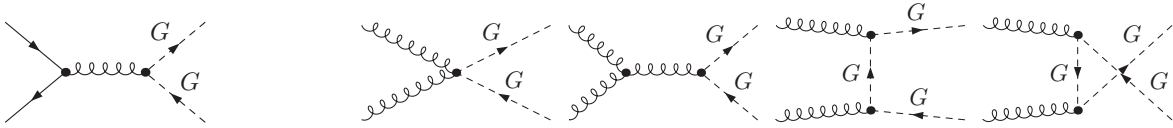


Figure 1: Leading order Feynman diagrams for sgluon pair production via quark-antiquark annihilation and gluon fusion.

two partonic LHC production mechanisms

$$q\bar{q} \rightarrow GG^* \quad \text{and} \quad gg \rightarrow GG^* \quad (1)$$

are shown in Figure 1. The sgluon coupling to gluons reads

$$\begin{aligned} \mathcal{L} \supset & D_\mu G^* D^\mu G - m_G^2 GG^* \\ & \supset -g_s f^{ABC} [G^{A*}(\partial^\mu G^B) - (\partial^\mu G^{A*})G^B] A_\mu^C + g_s^2 [f^{ACE} f^{BDE} + f^{ADE} f^{BCE}] G^{C*} G^D A_\mu^A A^{B\mu}. \end{aligned} \quad (2)$$

Incidentally, we notice the absence of direct sgluon couplings to matter. In supersymmetry they only arise as effective dimension-5 operators induced by the one-loop squark and gluino loops with a non-trivial scaling for individual heavy masses [1]. As long as these couplings are small — which is true if they are loop-induced — the sgluon mass range is not constrained by stringent bounds from dijet resonance searches. As a consequence, sgluons can be relatively light. Conversely, for $\mathcal{O}(1)$ sgluon-quark-quark couplings sgluon masses below $m_G = \mathcal{O}(2 \text{ TeV})$ are ruled out by the LHC experiments.

We implement the couplings shown in Eq.(2) into the MADGRAPH framework [27]. MADGOLEM then generates all tree-level diagrams and the corresponding helicity amplitudes, making use of MADGRAPH and HELAS [28]. All one-loop amplitudes and the corresponding helicity amplitudes we generate with a modified version of QGRAF [29] and GOLEM [30, 31]. The model specific ultraviolet counter terms are part of the model implementation. The subtraction of infrared and (if applicable) on-shell divergences is automatized [25, 32].

Throughout our analysis we use the CTEQ6L1 and CTEQ6M parton densities [33] with consistent values of α_s . For the central renormalization and factorization scales we choose the average final state mass $\mu^0 \equiv \mu_{R,F} = m_G$, which has been shown to lead to stable perturbative results [25, 26]. The LHC center of mass energy is $\sqrt{S} = 8 \text{ TeV}$. Unless stated otherwise, we set the sgluon mass to $m_G = 500 \text{ GeV}$.

Technically, there is a MADGRAPH4 [27] issue with the color structure of the quartic gluon-gluon-sgluon-sgluon coupling shown in Eq.(2). We therefore generate the required structure $f^{ACE} f^{BDE} + f^{ADE} f^{BCE}$ through an auxiliary massive, color-adjoint vector boson V_μ with an appropriate coupling to a gluon and a sgluon, namely

$$G^{A*} A_\mu^B V^{C\mu} : g_s m_V f^{ABC} \quad G^A A_\mu^B V^{C\mu} : -g_s m_V f^{ABC}. \quad (3)$$

The quartic gluon-sgluon interaction is then simply given by the decoupling limit $m_V^2 \gg s$. For MADGRAPH5 this technical complication is not necessary any longer.

Production rates to Next-to-Leading order

As a first step we present the results for the total NLO cross section for sgluon pair production. Later in this section we focus on more specific aspects of the real and virtual corrections. Unless stated otherwise, we assume $m_G = 500 \text{ GeV}$ and $\sqrt{S} = 8 \text{ TeV}$.

The size of the QCD quantum effects we describe in terms of the consistent factor $K \equiv \sigma^{\text{NLO}}/\sigma^{\text{LO}}$. From the production of supersymmetric particles it is well known that for LHC energies of 8 TeV and particle masses in the 500 GeV to 1 TeV mass range this correction factor can become unexpectedly large. This is not a sign of poor perturbative behavior but an artifact of the LO CTEQ parton densities [33, 34]. Correspondingly, Table I typically shows $K \gtrsim 1.5$ for this collider energy while the 14 TeV scenario has smaller, yet sizeable, corrections.

We then provide a comprehensive analysis of the LO and NLO cross sections $\sigma(pp \rightarrow GG^*)$ as a function of the sgluon mass in Fig. 2. In the left panel we show the LO and NLO cross sections with the envelope of the NLO factorization and renormalization scale variation in the range $\mu^0/2 < \mu_{R,F} < 2\mu^0$. The effects of an independent as well as diagonal variation of the factorization and renormalization scales we show in Fig. 3 and discuss below. As alluded to, the LO parton densities drive the LO cross sections to unexpectedly small values which makes the NLO corrections appear larger than $\sim 100\%$ for sgluon masses in the TeV range.

m_G [GeV]	$\sqrt{S} = 8$ TeV			$\sqrt{S} = 14$ TeV		
	σ^{LO} [pb]	σ^{NLO} [pb]	K	σ^{LO} [pb]	σ^{NLO} [pb]	K
200	2.12×10^2	3.36×10^2	1.58	9.77×10^2	1.48×10^3	1.52
350	8.16×10^0	1.36×10^1	1.66	5.44×10^1	8.46×10^1	1.56
500	7.64×10^{-1}	1.34×10^0	1.75	7.14×10^0	1.14×10^1	1.60
750	3.40×10^{-2}	6.54×10^{-2}	1.93	5.56×10^{-1}	9.29×10^{-1}	1.67
1000	2.47×10^{-3}	5.29×10^{-3}	2.15	7.31×10^{-2}	1.28×10^{-1}	1.75

Table I: Total $pp \rightarrow GG^*$ cross sections and corresponding K -factors for different sgluon masses and LHC energies.

In the right panel of Fig. 2 we separate the contributions stemming from the different partonic sub-channels: $q\bar{q}$, gg and the crossed purely NLO $gq/g\bar{q}$ initial state. The NLO corrections steadily increase for increasing sgluon masses. In part, we can trace back this behavior to threshold effects which we will further discuss below. The right panel of Fig. 2 also quantifies the dominance of the gluon-fusion mechanism $gg \rightarrow GG^*$. The reason is twofold: first, the color charges in the four-octet interaction are larger than the triplet-octet combination that drives the $q\bar{q}$ channel. Second, the gg channel benefits from particular kinematic features of the parton level process. While $q\bar{q} \rightarrow GG^*$ to LO proceeds merely through the (derivative) gGG coupling, the gg mechanism also receives a contribution from the (contact) quartic interaction. The first case corresponds to a p -wave and implies that the total (partonic) cross section scales as $\sigma_{q\bar{q}} \sim \beta^3$ at threshold, where $\beta = \sqrt{1 - 4m_G^2/s}$ denotes the sgluon velocity in the center-of-mass frame. In the gluon fusion case the s -wave component from the quartic interaction translates into a linear dependence $\sigma(gg) \sim \beta$. The latter dominates in the vicinity of the threshold which, moreover, corresponds to the low- x region where the gluon parton densities becomes large.

Following these arguments we can compare sgluon pair production to stop pair production (or squark pair production with decoupled gluinos) [26]. The differences at leading order can be traced to the relative strength of the color interactions arising from the fundamental vs adjoint final-state scalars. The ratios of the expected sgluon versus stop pair production rates can be roughly inferred from their parton level cross sections. We can compute these ratios directly from the corresponding analytical expressions [1, 2],

$$\frac{\sigma(q\bar{q} \rightarrow \tilde{t}\tilde{t}^*)}{\sigma(q\bar{q} \rightarrow GG^*)} = 1/6 \quad \frac{\sigma(gg \rightarrow \tilde{t}\tilde{t}^*)}{\sigma(gg \rightarrow GG^*)} \simeq 1/20. \quad (4)$$

These estimates nicely agree with the NLO results for stop pair production available from PROSPINO [26], which give $\sigma(pp \rightarrow \tilde{t}\tilde{t}^*) \sim 3$ pb for stop masses of $m_{\tilde{t}} \sim 350$ GeV, *i.e.* a factor of $\mathcal{O}(20)$ below the sgluon results in Table I and Fig. 2. The NLO effects to squark pair production are comparatively mild. In contrast, gluino pair production as an example of a color-octet interaction also shows large K factors and a very pronounced dependence on the mass of the produced heavy particles.

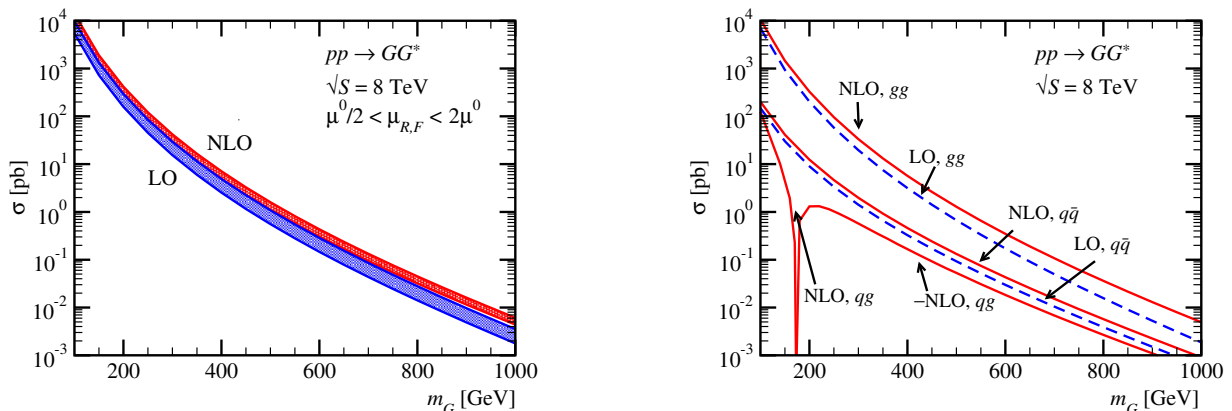


Figure 2: LO and NLO cross sections $\sigma(pp \rightarrow GG^*)$ as a function of the sgluon mass. The band corresponds to a scale variation $\mu^0/2 < \mu_{R,F} < 2\mu^0$. In the right panels we explicitly separate the contributions from the different partonic sub-channels, $q\bar{q}$, gg and also gq .

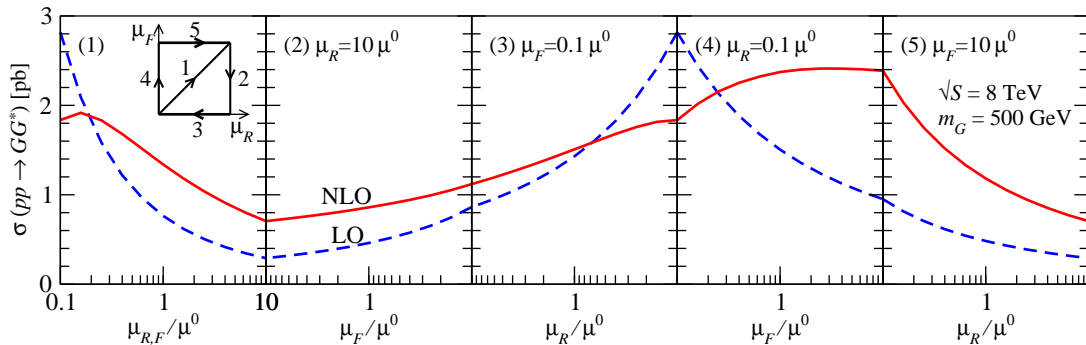


Figure 3: Renormalization and factorization scale dependence. The plot traces the scale dependence following a contour in the μ_F - μ_R plane in the range $\mu = (0.1 - 10) \times \mu^0$ with $\mu^0 = m_G$. The sgluon mass we fix to $m_G = 500$ GeV.

Scale dependence

Aside from the often positive corrections to the production rate the main motivation for the computation of higher order corrections is the reduced theoretical uncertainty. While we cannot derive the uncertainties arising from unknown higher orders in QCD from first principles, we can attempt to track them in the dependence of unphysical parameters introduced by the perturbative approach. An example for such a parameter are the factorization and renormalization scales which we introduce when we remove collinear and ultraviolet divergences order by order in perturbation theory. In the limit of infinitely many terms in the power series in α_s these scale dependences have to vanish, so unless there is a systematic shift from one perturbative order to the next the scale dependence should cover the asymptotic cross section values. While for Drell-Yan-type processes we know that this argument fails, purely color mediated processes with $\sigma^{\text{LO}} \propto \alpha_s^2$ tend to give a reasonable error estimate this way [25, 26]. Vice versa, we can at least firmly state that the scale variation gives a minimum uncertainty simply because we have the freedom to choose the two scales within a reasonable energy range.

In Fig. 3 we show the scale dependence for the $pp \rightarrow GG^*$ production rate, independently changing the renormalization (μ_R) and the factorization (μ_F) scales. We illustrate the path in two dimensions in the little square in the first panel. The individual scale variation is chosen as $\mu^{(0)}/10 < \mu < 10\mu^{(0)}$, where $\mu^{(0)}$ stands for our central value choice $\mu_F = \mu_R = \mu^{(0)} = m_G = 500$ GeV. The stabilization of the mentioned scale dependence manifests itself as a smoother σ^{NLO} slope, with varies typically around $\Delta\sigma^{\text{NLO}}/\sigma^{\text{NLO}} \sim \mathcal{O}(30\%)$, while for leading order this variation can be as large as $\mathcal{O}(80\%)$.

We also see that the maximum rate at small scale values which is often interpreted as a sign of scale stabilization is an artifact of identifying the two scales. An independent variation gives the largest rates at small values of the renormalization scale combined with larger values of the factorization scale — even though from a resummation point of view it is not clear how such a scale choice would be interpreted [24].

Real emission

Real emission corrections to sgluon pair production arise at order α_s^3 and originate from the three-particle final state contributions, wherein one extra gluon accompanies the produced sgluon pair. We show sample Feynman diagrams in Fig. 4. Following the standard procedure we subtract infrared divergences from the emitted gluon in the soft and/or collinear regimes using the massive Catani-Seymour dipoles [35, 36]. In addition to the SM dipoles available in the MADDIPOLE [37] package, MADGOLEM includes for example the sgluon dipoles to cope with our novel infrared divergent structure. Such divergences appear when the external sgluons radiate soft gluons and require new final-final and final-initial dipoles. The sgluon can also be a heavy spectator parton, but for this case we can simply use the SM initial-final dipoles. This is because for the dipole function the spectator carries information about the mass of the colored particle, but not about its spin.

In Appendix A we give the new sgluon dipoles including the FKS-style phase space cutoff $0 < \alpha \leq 1$ [38]. The numerical implementation is publicly available upon request. Among several numerical improvements, the parameter α gives us an easy handle to check our implementation. For a wide range $\alpha = 10^0 - 10^{-8}$ we find stable cross section for the combination of the real emission diagrams with the integrated dipoles. As a default value in MADGOLEM we use $\alpha = 10^{-3}$.

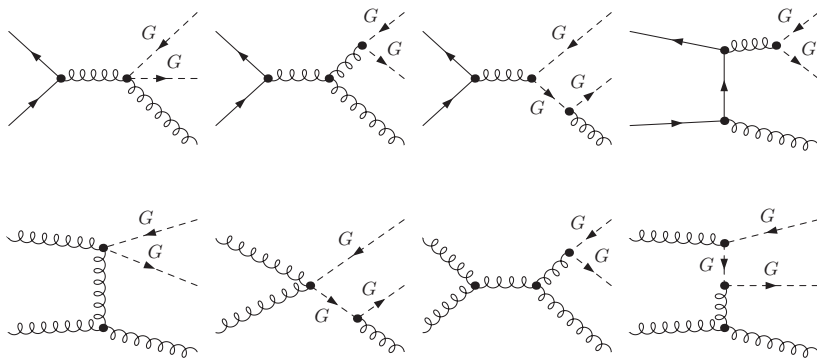


Figure 4: Sample Feynman diagrams for real emission corrections to sgluon pair production via quark-antiquark annihilation (upper) and gluon fusion (lower).

Virtual corrections

Virtual corrections to sgluon pair production appear as order α_s^3 contributions from virtual gluons coupling to quarks and sgluons. All divergences we regularize in $n = 4 - 2\epsilon$ dimensions. The infrared poles are cancelled after we include the integrated Catani-Seymour dipoles [35, 36] and take into account the collinear higher order correction consistently included in the definition of the parton densities. The ultraviolet divergences are absorbed in the physical renormalization of the strong coupling constant and the sgluon mass. As described in Appendix B we use the $\overline{\text{MS}}$ scheme with decoupled heavy colored states [39] for the strong coupling and the on-shell scheme for the mass. For an internal check we use an independent implementation of our sgluon model in FEYNARTS; all MADGOLEM results can then be numerically compared to the output from FEYNARTS, FORMCALC and LOOPTOOLS [40].

Starting with the dominant gluon fusion channel, in the left panel of Fig. 6 we examine different contributions to the real and virtual NLO corrections to the hadronic process $pp \rightarrow GG^*$ as a function of the sgluon mass. Leaving aside gauge invariance issues while applying a numerical test we separately show different one-loop pieces normalized to the LO rate, $\Delta\sigma^{\text{NLO}}/\sigma^{\text{LO}}$. In addition, we distinguish the partonic subprocesses $q\bar{q}$ and gg . The crossed channel qg does not develop any virtual corrections but is required for the complete cancellation of the collinear divergence.

The real emission together with the virtual box diagrams contributes the bulk of the NLO quantum effects. Both feature a characteristic growing trend with increasing sgluon mass. For intermediate sgluon masses, real emission gives rise to corrections in the ballpark of 20 – 60%, but it may eventually reach up to 100% for TeV-scale sgluons. Note that this behavior cannot be interpreted as a break-down of perturbation theory because QCD corrections to our supersymmetric setup are fundamentally well defined. Box-like topologies, *i.e.* one-loop corrections to the $ggGG$ vertex including diagrams shown as the 3th and 4th diagrams in the lower row of Fig. 5, amount to roughly 40% and exhibit a slightly milder dependence on m_G . Both, the size of these contributions and their increase with m_G we can attribute to the peculiar threshold behavior of the NLO corrections. In particular, long-range gluon exchange

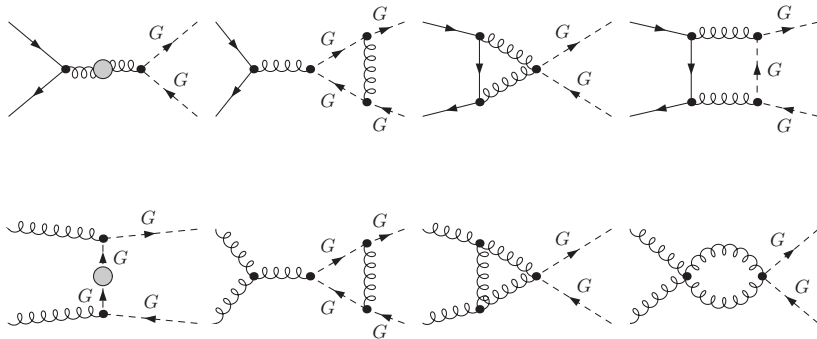


Figure 5: Sample Feynman diagrams for virtual corrections to sgluon pair production via quark-antiquark annihilation (upper) and gluon fusion (lower).

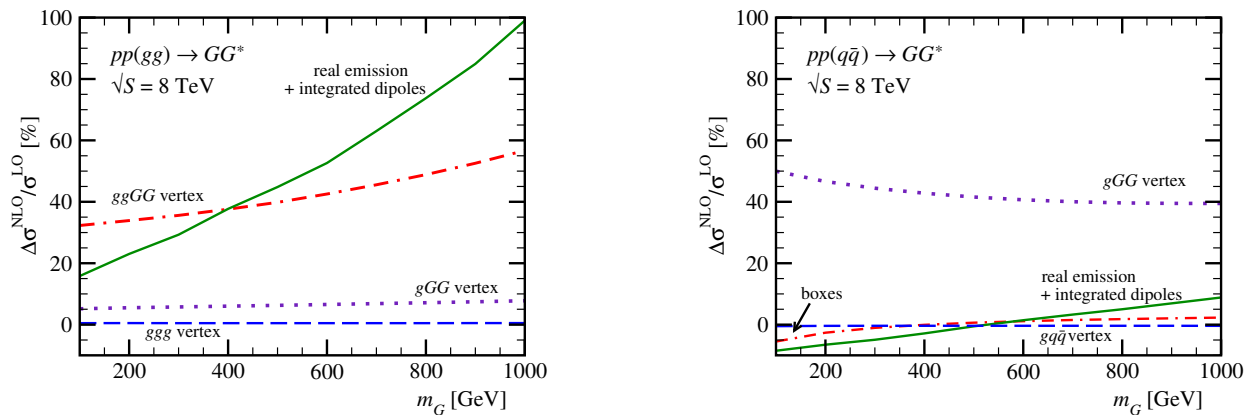


Figure 6: Relative size $\Delta\sigma^{\text{NLO}}/\sigma^{\text{LO}} \equiv (\sigma^{\text{NLO}} - \sigma^{\text{LO}})/\sigma^{\text{LO}}$ of the real emission and virtual corrections to $\sigma(pp \rightarrow GG^*)$ as a function of the sgluon mass m_G . We separate the partonic gg (left) and $q\bar{q}$ (right) initial states. The contribution from the self-energies is negligible and not explicitly shown.

between slowly moving heavy final-state particles $\beta \rightarrow 0$ develops a Coulomb singularity $\sigma^{\text{NLO}} \sim \pi\alpha_s/\beta$ which cancels the linear dependence from the tree-level contribution $\sigma^{\text{LO}} \sim \beta$ and leads to a finite NLO rate but a divergent K factor [26]. Gluon radiation off the initial state carries positive, and potentially large, logarithmic pieces which supply an additional source of enhancement – and that can eventually be resummed [9].

For the subleading $q\bar{q}$ initial state we find a sizable contribution from the gluon-sgluon-sgluon gGG vertex corrections. They are fairly independent of variations of the sgluon mass. The remaining one-loop topologies only contribute at the percent level of less.

III. DISTRIBUTIONS: NLO VERSUS MULTI-JET MERGING

Predictions based on (fixed-order) NLO cross sections entail significant improvements of the central values and the theory uncertainties, as we have just shown for the specific case $pp \rightarrow GG^*$. Before these results can be integrated in experimental analyses we need to confirm that this quantitative picture also holds for the main distributions. Previous work in the literature shows that the transverse momentum and rapidity distributions of pair produced heavy particles are relatively stable with respect to higher-order corrections [22, 25]. For the production of such heavy particles a parton shower should deliver a good description of jet radiation patterns, because its underlying collinear approximation applies for a wide range of transverse momenta relative to the sgluon masses [1, 41, 42]. Normalizing the event numbers generated by standard Monte Carlo tools to the NLO cross section should therefore be an appropriate strategy.

To quantitatively assess such statements we compare the fixed order NLO parton-level distributions for the production process $pp \rightarrow GG^*$, as obtained from MADGOLEM, with a multi-jet merging calculation. For the latter we employ the MLM [23] scheme and generate events using MADGRAPH 4.5 [42] interfaced with PYTHIA [43]. The entire description of our sgluon is supplied by the MADGOLEM model file. In Fig. 7 we display the resulting transverse momentum and rapidity distributions for one outgoing sgluon for the NLO calculations as well as for jet merging including up to two hard jets. Only including one hard jet in the merging prescription would not change the results within their numerical precision. Those two distributions are normalized to unity. For the NLO results we separately show the LO, real emission, and virtual gluon contributions, defined in terms of Catani-Seymour dipoles with $\alpha = 10^{-3}$.

First, we see that all different ingredients of the NLO distributions have essentially the same shapes. Large effects on the total rate from collinear radiation or Coulomb singularities only have a negligible effect on the distributions of the heavy states. In addition, the normalized fixed-order and merged distributions agree very well. Small differences like the slightly harder p_T profile of the merged prediction are accounted for by the extra recoil jets from the parton shower. Similarly, such a second jet from initial state radiation can balance the first emission and lead to more central sgluons in the detector.

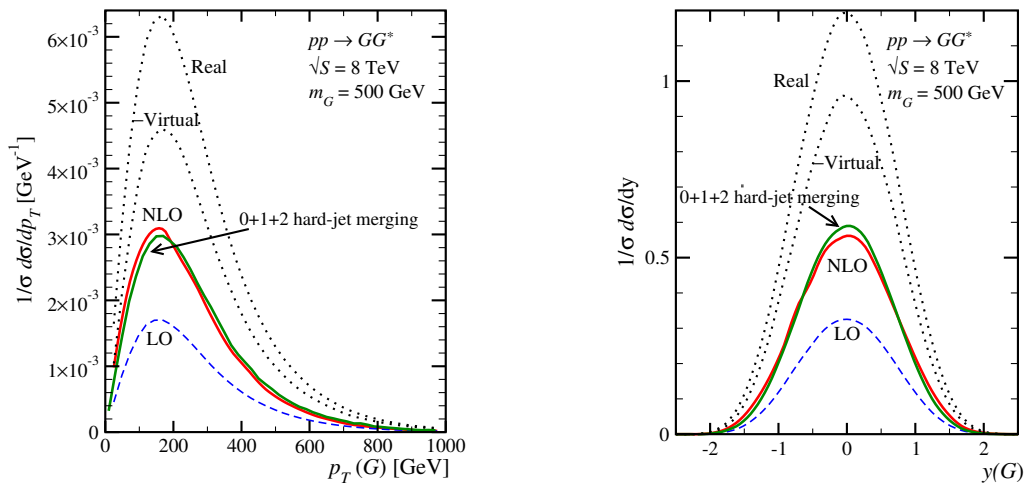


Figure 7: Sgluon transverse momentum and rapidity distributions at parton level. We assume $m_G = 500$ GeV and $\sqrt{S} = 8$ TeV. For the NLO curves we separately display the LO, virtual, and real contributions ($\alpha = 10^{-3}$). In addition, we show the corresponding distributions based on multi-jet merging in the MLM scheme [23] with up to two hard radiation jets. The NLO and merged results are normalized to unity while the different contributions to the NLO rates are shown to scale.

IV. SUMMARY

We report on the first complete calculation of sgluon pair production to next-to-leading order. The pairwise production of scalar color-adjoints we define in terms of an extended supersymmetric model; however, after decoupling squarks and gluinos our results can be considered reasonably model-independent. The sgluons have tree level QCD couplings to gluons and do not couple to matter. We find

1. potentially large production rates, driven by the gluon fusion subprocess. Typical numbers range around $\sigma \sim \mathcal{O}(1 \text{ pb})$ for sgluon masses of $m_G \simeq 500$ GeV and $\sqrt{S} = 8$ TeV. Such small masses are not ruled out by current experimental constraints.
2. sizable NLO quantum effects, traced back to real gluon radiation and a certain subsets of vertex and box virtual corrections. Their relative size increases with the sgluon mass, mainly due to threshold effects.
3. substantially reduced theoretical uncertainties. The scale dependence which is dominated by the renormalization scale choice and which may reach $\mathcal{O}(80\%)$ at leading order, is reduced by a factor $1/2 - 1/4$.
4. NLO sgluon distributions which agree very well with complementary results from multi-jet merging. Applying the NLO rate normalization to sgluons+jets event generation should give very consistent predictions for the LHC.

Besides its phenomenological impact our study illustrates the performance of the (soon-to-be-public) MADGOLEM package. The genuine dipole and counter term structures which cope with infrared and ultraviolet divergences in the presence of the sgluon field have been implemented and can be accessed automatically. In this sense the present study qualifies as a non-trivial example of a fully automatized NLO calculation for the production of heavy particles beyond the Standard Model.

Acknowledgments

KM and IW would like to thank the Institute for Theoretical Physics and Heidelberg University for their support and hospitality during many visits. DG acknowledges support by the International Max Planck Research School for Precision Tests of Fundamental Symmetries. This work is in part supported by the Concerted Research action ‘‘Supersymmetric Models and their Signatures at the Large Hadron Collider’’ of the Vrije Universiteit Brussel and by the Belgian Federal Science Policy Office through the Interuniversity Attraction Pole IAP VI/11.

Appendix A: Sgluon dipoles

Sgluons are color octets with spin zero, so their dipoles are identical to supersymmetric scalar quarks with modified color factors $C_F \rightarrow C_A$. To remove the related infrared divergences we implement the (un)integrated dipoles presented in Appendix C of Ref. [36] with this replacement. In addition, we introduce a variable size of the subtraction phase space, $0 < \alpha \leq 1$, as pioneered in the FKS subtraction scheme [38]. Values $\alpha < 1$ limit the phase space region over which we subtract finite dipole contributions around the soft-collinear pole. Our notation closely follows Ref. [36].

From Eq.(C.1) of Ref. [36] we obtain the sgluon dipole function $\langle V_{gG,k} \rangle$ for the final-final case. The corresponding integrated dipole is decomposed into an eikonal part including the soft integrals and the remaining hard collinear integrals,

$$I_{gG,k} = C_A [2I^{\text{eik}} + I_{gG,k}^{\text{coll}}] . \quad (\text{A1})$$

The divergent and finite parts of the regularized eikonal and collinear integrals in $4 - 2\varepsilon$ dimensions are

$$\begin{aligned} \tilde{v}_{gG,k} I^{\text{eik}} &= \frac{1}{2\varepsilon^2} \left(1 - (\mu_G + \mu_k)^2\right)^{-2\varepsilon} \left(1 - \frac{\rho_G^{-2\varepsilon}}{2} - \frac{\rho_k^{-2\varepsilon}}{2}\right) \\ &\quad + \frac{\zeta_2}{4} (6 - \mu_G^{-2\varepsilon} - \mu_k^{-2\varepsilon}) + 2\text{Li}_2(-\rho) - 2\text{Li}_2(1-\rho) - \frac{1}{2}\text{Li}_2(1-\rho_G^2) - \frac{1}{2}\text{Li}_2(1-\rho_k^2) \Big] \\ I_{gG,k}^{\text{coll}} &= \frac{2}{\varepsilon} - \frac{\mu_G^{-2\varepsilon}}{\varepsilon} - 2\mu_G^{-2\varepsilon} + 6 - 2\log\left((1-\mu_k)^2 - \mu_G^2\right) + \frac{4\mu_k(\mu_k-1)}{1-\mu_G^2-\mu_k^2}, \end{aligned} \quad (\text{A2})$$

where the rescaled mass μ_n and the variables ρ and ρ_n , associated with the splitting $\tilde{i}j \rightarrow ij$ and the spectator k , are defined using the final state momenta p_i, p_j and p_k

$$\begin{aligned} \mu_n &= \frac{m_n}{\sqrt{Q^2}} && \text{with } Q^\mu = p_i^\mu + p_j^\mu + p_k^\mu \\ \rho &= \sqrt{\frac{1 - \tilde{v}_{ij,k}}{1 + \tilde{v}_{ij,k}}} && \text{with } \tilde{v}_{ij,k} = \frac{\sqrt{\lambda(1, \mu_{ij}^2, \mu_k^2)}}{1 - \mu_{ij}^2 - \mu_k^2} \\ \rho_n(\mu_j, \mu_k) &= \sqrt{\frac{1 - \tilde{v}_{ij,k} + 2\mu_n^2/(1 - \mu_j^2 - \mu_k^2)}{1 + \tilde{v}_{ij,k} + 2\mu_n^2/(1 - \mu_j^2 - \mu_k^2)}} \quad (n = j, k) . \end{aligned} \quad (\text{A3})$$

The kinematics of the splitting is described by

$$\tilde{z}_j = 1 - \frac{p_i p_k}{p_i p_k + p_j p_k} \quad y_{ij,k} = \frac{p_i p_j}{p_i p_j + p_i p_k + p_j p_k}, \quad (\text{A4})$$

where the upper limit in the $y_{ij,k}$ phase space integration is

$$y_+ = 1 - \frac{2\mu_k(1-\mu_k)}{1-\mu_i^2-\mu_j^2-\mu_k^2}. \quad (\text{A5})$$

To include the phase space parameter α in the unintegrated dipole we simply add the step function $\Theta(\alpha - y_{gG,k}/y_+)$. It ensures that only for $y_{gG,k} < \alpha y_+$ instead of the entire range $y_{gG,k} < y_+$ the dipole is subtracted from the hard matrix element. For the integrated dipole part we modify Eq.(A1) by subtracting the finite phase space contributions which a choice of $\alpha \neq 1$ removes,

$$\begin{aligned} I_{gG,k}(\alpha) &= I_{gG,k} - \Delta I_{gG,k}(\alpha) \\ &= I_{gG,k} - \frac{2\pi}{\alpha_s} \int [dp_g(\tilde{p}_{gG}, \tilde{p}_k)] \Theta\left(\frac{y_{gG,k}}{y_+} - \alpha\right) \frac{\langle V_{gG,k} \rangle}{2p_g p_G}. \end{aligned} \quad (\text{A6})$$

For the (by definition) finite contribution $\Delta I_{gG,k}$ we set $\varepsilon = 0$. The eikonal part of the kernel $2/[1 - \tilde{z}_G(1 - y_{gG,k})]$ is the same for the $\langle V_{gQ,k} \rangle$ and $\langle V_{gG,k} \rangle$, so we use the SM result for $\Delta I^{\text{eik}}(\alpha)$ as provided in Eq.(A.9) of Ref. [44]. The collinear part is different, giving a correction to Eq.(A1) of the form

$$- \Delta I_{gG,k}(\alpha) = -C_A \left[2\Delta I^{\text{eik}}(\alpha) + \frac{1}{2\pi^2} \left(\frac{(1-\mu_k)^2 - \mu_G^2}{1-\mu_G^2-\mu_k^2} (1-\alpha) + \log \alpha \right) \right]. \quad (\text{A7})$$

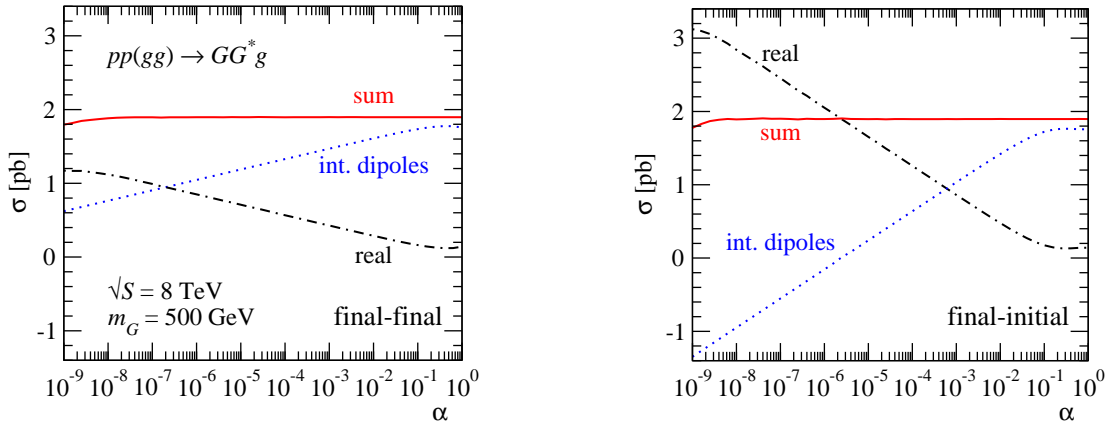


Figure 8: α dependence of the final-final (left) and final-initial (right) sgluon dipoles for the sub-process $gg \rightarrow GG^*g$.

As expected, this result becomes trivial for $\alpha = 1$ and diverges in the limit $\alpha \rightarrow 0$.

For the final-initial dipole function we start from Eq.(C.3) of Ref. [36] which gives rise to the regularized integrated dipole function

$$I_{gG}^a(x) = C_A \left[J_{gG}^a(x)_+ + \delta(1-x) \left(J_{gG}^{a;S} + J_{gG}^{a;NS} \right) \right]. \quad (\text{A8})$$

The three contributions to I_{gG}^a are

$$\begin{aligned} J_{gG}^a(x)_+ &= \left(\frac{-2 - 2 \log(1-x + \mu_G^2)}{1-x} \right)_+ + \left(\frac{2}{1-x} \right)_+ \log(2 + \mu_G^2 - x) \\ J_{gG}^{a;S} &= \frac{1}{\varepsilon^2} - 2\zeta_2 - \mu_G^{-2\varepsilon} \left(\frac{1}{\varepsilon^2} + \frac{1}{\varepsilon} + \zeta_2 + 2 \right) - \frac{1}{\varepsilon} \log(1 + \mu_G^2) + \left(\frac{2}{\varepsilon} + 4 - \zeta_2 \right) \\ J_{gG}^{a;NS} &= 2\zeta_2 - 2\text{Li}_2 \left(\frac{1}{1 + \mu_G^2} \right) - 2\text{Li}_2(-\mu_G^2) - \frac{1}{2} \log^2(1 + \mu_G^2) \end{aligned} \quad (\text{A9})$$

Again, we introduce an α parameter into the unintegrated phase space integration, limiting the application of the dipole subtraction to the region $1 - x_{gG,a} < \alpha$. The kinematical variable $x_{ij,a}$ is given by

$$x_{ij,a} = \frac{p_a p_i + p_a p_j - p_i p_j + \frac{1}{2} (m_{ij}^2 - m_i^2 - m_j^2)}{p_a p_i + p_a p_j}. \quad (\text{A10})$$

The additional contribution to the integrated dipole I_{gG}^a shown in Eq.(A8) is

$$\Delta I_{gG}^a(\alpha) = C_A \frac{\Theta(1-\alpha-x)}{1-x} \left(-2 + 2 \log \left(1 + \frac{1}{1 + \mu_G^2 - x} \right) \right) \quad (\text{A11})$$

Again, this result becomes trivial for $\alpha = 1$ and diverges in the limit of $\alpha \rightarrow 0$ now when performing the integral over x .

The numerical effects of a variable α parameter on the subprocess $gg \rightarrow GG^*g$ we show in Fig. 8. While the individual unintegrated and integrated dipole contributions diverge logarithmically with small α the sum of them is numerically stable over eight orders of magnitude. This kind of test is sensitive to many aspects of our calculation, namely the proper coverage of all divergences, the relative normalization of the two and three particle phase space, etc. In Fig. 8 we see that a default value of $\alpha = 10^{-3}$ gives roughly equal contributions from unintegrated and integrated dipoles, avoiding large numerical cancellations for the final-initial dipole. For the final-final dipole we would have to go to smaller values of α which make the final-initial case harder, so we use $\alpha = 10^{-3}$ throughout.

Appendix B: Renormalization

The ultraviolet counter terms we include automatically via the leading-order QGRAF output. At present, MAD-GOLEM fully supports the calculation of NLO QCD corrections for the Standard Model, the MSSM, and several



Figure 9: Feynman diagrams for the sgluon field renormalization (left) and sgluon-mediated gluon field renormalization (right).

other extensions of the Standard Model, including sgluons. For dimensional regularization we employ the standard 't Hooft-Veltman scheme with $n = 4 - 2\varepsilon$ dimensions. The renormalization constants we define through the additive or multiplicative relations between the bare and the renormalized fields,

$$\Psi^{(0)} \rightarrow Z_\Psi^{1/2} \Psi \quad m_\Psi^{(0)} \rightarrow m_\Psi + \delta m_\Psi \quad g_s^{(0)} \rightarrow g_s + \delta g_s \quad (\text{with } \Psi = q, A, G). \quad (\text{B1})$$

These field, mass and coupling renormalization constants we conventionally phrase in terms of two-point functions which we supply in a separate library. Given a generic Lagrangian $\mathcal{L}(\Psi, m_\Psi, g_s)$ with a QCD interaction this consistently gives a counter term Lagrangian of the form $\delta\mathcal{L}(\Psi, m_\Psi, g_s, \delta\Psi, \delta m_\Psi, \delta g_s)$.

First of all, a new sgluon field modifies the strong beta function. If we start with the quantum corrections to the quark-quark-gluon vertex in terms of the strong coupling Z_{g_s} , the gluon field renormalization Z_3 , and the quark field renormalization Z_2 this translates into a combined $Z_1 = Z_{g_s} Z_2 Z_3^{1/2}$. Each of these renormalization constants we expand as $Z_i = 1 + \delta_i + \mathcal{O}(\alpha_s^2)$, with $\overline{\text{MS}}$ counter terms δ_i . The strong coupling constant renormalization at one loop we can thus write as

$$\begin{aligned} \delta g_s &= \delta_1 - \delta_2 - \frac{1}{2}\delta_3 \\ \text{with } \delta_1 &= \delta_1^{\text{SM}} = -\frac{\alpha_s}{4\pi} (C_A + C_F) \Delta_\varepsilon \\ \delta_2 &= \delta_2^{\text{SM}} = -\frac{\alpha_s}{4\pi} C_F \Delta_\varepsilon \\ \delta_3 &= \delta_3^{\text{SM}} + \delta_3^G = \frac{\alpha_s}{4\pi} \left(\frac{5}{3} C_A - n_f C_F T_R \right) - \frac{\alpha_s}{12\pi} C_A \Delta_\varepsilon. \end{aligned} \quad (\text{B2})$$

The shifted pole in the $\overline{\text{MS}}$ prescription is $\Delta_\varepsilon = 1/\varepsilon - \gamma_E + \log(4\pi)$ and the active number of fermions is $n_f = 6$. Because there are no direct couplings between sgluons and matter fields δ_2 keeps its SM value. For the same reason, sgluon-mediated corrections to the quark-quark-gluon vertex are absent at one loop, so δ_1 does not change. Only the gluon self energy is modified by the triple and quartic gluon/sgluon interactions, as displayed in Fig. 9.

Combining all of the above contributions and decoupling the heavy (H) colored degrees of freedom — in our case the top and the sgluon — gives us the final expression for δg_s in terms of the measured α_s values. We implement this subtraction in the zero-momentum scheme [25, 39]. It leaves the renormalization group running of α_s merely determined by the light (L) degrees of freedom. The renormalization constant finally reads

$$\begin{aligned} \delta g_s &= -\frac{\alpha_s}{4\pi} \frac{\beta_0^L + \beta_0^H}{2} \Delta_\varepsilon - \frac{\alpha_s}{4\pi} \left(\frac{1}{3} \log \frac{m_t^2}{\mu_R^2} + \frac{1}{2} \log \frac{m_G^2}{\mu_R^2} \right) \\ \beta_0 &= \beta_0^L + \beta_0^H = \left(\frac{11}{3} C_A - (n_f - 1) C_F T_R \right) - \left(C_F T_R + \frac{1}{3} C_A \right). \end{aligned} \quad (\text{B3})$$

In a second step we need to compute the QCD renormalization constants in the sgluon sector. The sgluon two-point function receives $\mathcal{O}(\alpha_s)$ corrections due to virtual gluon interchange, as shown in Fig. 9. The corresponding ultraviolet divergences we absorb into the sgluon mass m_G and field-strength Z_G . As renormalization condition we choose the on-shell scheme

$$\begin{aligned} \Re \hat{\Sigma}'(m_G^2) &= 0 \quad \Rightarrow \quad \delta Z_G = -\Re \Sigma'(m_G^2) \\ \Re \hat{\Sigma}(m_G^2) &= 0 \quad \Rightarrow \quad \delta m_G = +\Re \Sigma(m_G^2), \end{aligned} \quad (\text{B4})$$

where $\Re \hat{\Sigma}_G$ denotes the (real part of the) renormalized sgluon self-energy,

$$\hat{\Sigma}_G(q^2) = \Sigma_G(q^2) + (q^2 - m_G^2) \delta Z_G - \delta m_G^2, \quad (\text{B5})$$

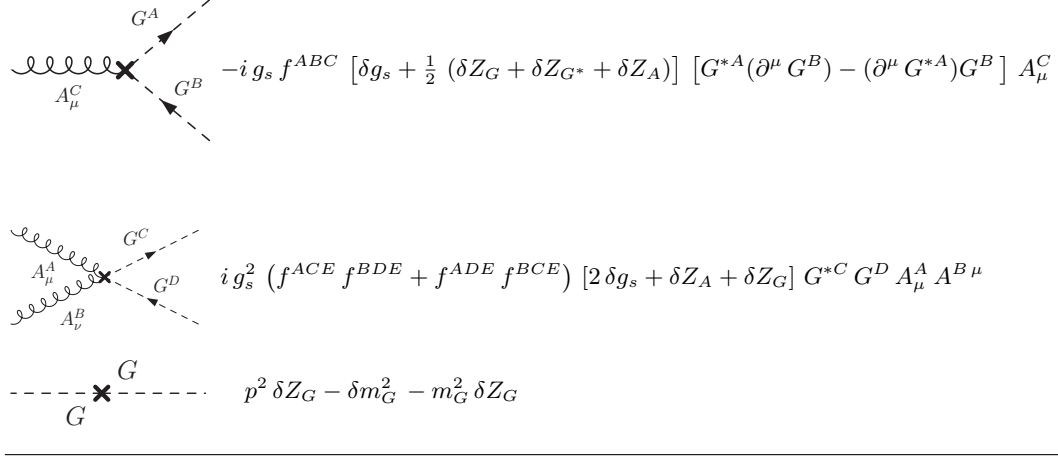


Table II: Counter term Feynman rules for the sgluon-mediated interactions.

and $\hat{\Sigma}'(q^2) \equiv d^2/dq^2 \hat{\Sigma}(q^2)$ the corresponding derivative with respect to the momentum squared. The analytic form of all renormalization constants we reduce down to one and two-point scalar loop integrals [45]. The sgluon mass and field strength renormalization then reads

$$\begin{aligned} \delta Z_G &= \frac{\alpha_s}{2\pi} C_A [B_0(m_G^2, m_G^2, 0) + m_G^2 B'_0(m_G^2, m_G^2, 0)] \\ \delta m_G &= -\frac{\alpha_s}{\pi} C_A \left[m_G^2 + \frac{3}{4} A_0(m_G^2) \right]. \end{aligned} \quad (\text{B6})$$

As expected, these expressions are identical to the squark case, modulo a factor C_A/C_F that reflects the different $SU_C(3)$ representations.

Finally, in Table II we quote the analytical expressions for the relevant ultraviolet counter terms $\delta\mathcal{L}$ as a function of the field, mass, and strong coupling renormalization constants derived in this Appendix.

-
- [1] T. Plehn and T. M. P. Tait, J. Phys. G **36**, 075001 (2009).
 - [2] S. Y. Choi, M. Drees, A. Freitas, and P. M. Zerwas, Phys. Rev. D **78**, 095007 (2008); S. Y. Choi, M. Drees, J. Kalinowski, J. M. Kim, E. Popeno, and P. M. Zerwas, Phys. Lett. B **672**, 246 (2009); S. Y. Choi, D. Choudhury, A. Freitas, J. Kalinowski, J. M. Kim, and P. M. Zerwas, JHEP **1008**, 025 (2010).
 - [3] D. E. Morrissey, T. Plehn, and T. M. P. Tait, Phys. Rep. in print, arXiv:0912.3259 [hep-ph].
 - [4] L. J. Hall and L. Randall, Nucl. Phys. B **352**, 289 (1991); G. D. Kribs, E. Poppitz, and N. Weiner, Phys. Rev. D **78**, 055010 (2008); S. D. L. Amigo, A. E. Blechman, P. J. Fox, and E. Poppitz, JHEP **0901**, 018 (2009); A. E. Blechman, Mod. Phys. Lett. A **24**, 633 (2009); R. Fok and G. D. Kribs, Phys. Rev. D **82**, 035010 (2010); S. Y. Choi, D. Choudhury, A. Freitas, J. Kalinowski, and P. M. Zerwas, Phys. Lett. B **697**, 215 (2011) [Erratum-ibid. B **698**, 457 (2011)].
 - [5] P. J. Fox, A. E. Nelson, and N. Weiner, JHEP **0208**, 035 (2002); Z. Chacko, P. J. Fox, and H. Murayama, Nucl. Phys. B **706**, 53 (2005); G. D. Kribs and A. Martin, arXiv:1203.4821 [hep-ph].
 - [6] I. Antoniadis, K. Benakli, A. Delgado, and M. Quirós, Adv. Stud. Theor. Phys. **2** (2008) 645 L. Mazzucato, Y. Oz, and S. Yankielowicz, JHEP **0711**, 094 (2007) K. Benakli and M. D. Goodsell, Nucl. Phys. B **816**, 185 (2009); K. Benakli and M. D. Goodsell, Nucl. Phys. B **840**, 1 (2010).
 - [7] C. Kilic, T. Okui and R. Sundrum, JHEP **1002**, 018 (2010); C. Kilic and T. Okui, JHEP **1004**, 128 (2010);
 - [8] G. Burdman, B. A. Dobrescu and E. Pontón, Phys. Rev. D **74**, 075008 (2006).
 - [9] A. Idilbi, C. Kim, and T. Mehen, Phys. Rev. D **79**, 114016 (2009).
 - [10] S. P. Martin, In *Kane, G.L. (ed.): Perspectives on supersymmetry II* 1-153 [hep-ph/9709356]; M. V. Martynov and A. D. Smirnov, Mod. Phys. Lett. A **23**, 2907 (2008); B. Fuks, [arXiv:1202.4769 [hep-ph]].
 - [11] see e.g. P. Fileviez Pérez, R. Gavin, T. McElmurry, and F. Petriello, Phys. Rev. D **78**, 115017 (2008).
 - [12] B. A. Dobrescu, K. Kong, and R. Mahbubani, JHEP **0707**, 006 (2007); B. A. Dobrescu, K. Kong, and R. Mahbubani, Phys. Lett. B **670**, 119 (2008).

- [13] M. I. Gresham and M. B. Wise, Phys. Rev. D **76**, 075003 (2007); M. Gerbush, T. J. Khoo, D. J. Phalen, A. Pierce, and D. Tucker-Smith, Phys. Rev. D **77**, 095003 (2008); M. V. Martynov and A. D. Smirnov, Mod. Phys. Lett. A **23**, 2907 (2008).
- [14] A. V. Manohar and M. B. Wise, Phys. Rev. D **74**, 035009 (2006); C. P. Burgess, M. Trott, and S. Zuberi, JHEP **0909**, 082 (2009); A. Idilbi, C. Kim, and T. Mehen, Phys. Rev. D **82**, 075017 (2010).
- [15] see e.g. R. S. Chivukula, A. Farzinnia, E. H. Simmons and R. Foadi, Phys. Rev. D **85**, 054005 (2012).
- [16] Y. Bai and B. A. Dobrescu, JHEP **1107**, 100 (2011).
- [17] Y. Bai and J. Shelton, arXiv:1107.3563 [hep-ph].
- [18] R. S. Chivukula, M. Golden and E. H. Simmons, Nucl. Phys. B **363**, 83 (1991); C. Kilic, T. Okui and R. Sundrum, JHEP **0807**, 038 (2008); C. Kilic, S. Schumann, and M. Son, JHEP **0904**, 128 (2009); T. Han, I. Lewis, and Z. Liu, JHEP **1012**, 085 (2010).
- [19] S. Schumann, A. Renaud, and D. Zerwas, JHEP **1109**, 074 (2011); G. Aad *et al.* [ATLAS Collaboration], Eur. Phys. J. C **71**, 1828 (2011); J. M. Arnold and B. Fornal, arXiv:1112.0003 [hep-ph].
- [20] A. R. Zerwekh, C. O. Dib, and R. Rosenfeld, Phys. Rev. D **77**, 097703 (2008).
- [21] C. Kim and T. Mehen, Phys. Rev. D **79**, 035011 (2009).
- [22] T. Binoth, D. Gonçalves Netto, D. López-Val, K. Mawatari, T. Plehn, and I. Wigmore, Phys. Rev. D **84**, 075005 (2011).
- [23] M. L. Mangano, M. Moretti, and R. Pittau, Nucl. Phys. B **632**, 343 (2002).
- [24] for a pedagogical introduction see e.g. T. Plehn, Lect. Notes Phys. **844**, 1 (2012) [arXiv:0910.4182 [hep-ph]].
- [25] W. Beenakker, R. Höpker, M. Spira, and P. M. Zerwas, Phys. Rev. Lett. **74**, 2905 (1995); W. Beenakker, R. Höpker, M. Spira and P. M. Zerwas, Nucl. Phys. B **492**, 51 (1997).
- [26] W. Beenakker, M. Krämer, T. Plehn, M. Spira and P. M. Zerwas, Nucl. Phys. B **515**, 3 (1998).
- [27] J. Alwall *et al.*, JHEP **0709**, 028 (2007).
- [28] H. Murayama, I. Watanabe and K. Hagiwara, KEK-91-11.
- [29] P. Nogueira, J. Comput. Phys. **105**, 279 (1993).
- [30] G. Cullen, N. Greiner, A. Guffanti, J. -P. Guillet, G. Heinrich, S. Karg, N. Kauer and T. Kleinschmidt *et al.*, Nucl. Phys. Proc. Suppl. **205-206**, 67 (2010); N. Greiner, A. Guffanti, T. Reiter and J. Reuter, Phys. Rev. Lett. **107**, 102002 (2011).
- [31] T. Binoth, J. P. Guillet, G. Heinrich, E. Pilon, and T. Reiter, Comput. Phys. Commun. **180**, 2317 (2009); G. Cullen, J. P. Guillet, G. Heinrich, T. Kleinschmidt, E. Pilon, T. Reiter and M. Rodgers, Comput. Phys. Commun. **182**, 2276 (2011).
- [32] T. Plehn, C. Weydert, PoS **CHARGED2010**, 026 (2010) [arXiv:1012.3761 [hep-ph]].
- [33] J. Pumplin, D. R. Stump, J. Huston, H. L. Lai, P. Nadolsky, and W. K. Tung, JHEP **0207**, 012 (2002).
- [34] Prospino collaboration, private communication.
- [35] S. Catani and M. H. Seymour, Phys. Lett. B **378**, 287 (1996); S. Catani and M. H. Seymour, Nucl. Phys. B **485**, 291 (1997) [Erratum-ibid. B **510**, 503 (1998)].
- [36] S. Catani, S. Dittmaier, M. H. Seymour and Z. Trocsanyi, Nucl. Phys. B **627**, 189 (2002).
- [37] R. Frederix, T. Gehrmann, and N. Greiner, JHEP **0809**, 122 (2008); and JHEP **1006**, 086 (2010).
- [38] S. Frixione, Z. Kunszt, and A. Signer, Nucl. Phys. B **467**, 399 (1996); Z. Nagy and Z. Trocsanyi, Phys. Rev. D **59**, 014020 (1999) [Erratum-ibid. D **62**, 099902 (2000)].
- [39] J. C. Collins, F. Wilczek, and A. Zee, Phys. Rev. D **18**, 242 (1978); S. Berge, W. Hollik, W. M. Möhle, and D. Wackerroth, Phys. Rev. D **76**, 034016 (2007).
- [40] T. Hahn, Comput. Phys. Commun. **140**, 418 (2001); T. Hahn and M. Pérez-Victoria, Comput. Phys. Commun. **118**, 153 (1999); T. Hahn and C. Schappacher, Comput. Phys. Commun. **143**, 54 (2002); T. Hahn and M. Rauch, Nucl. Phys. Proc. Suppl. **157**, 236 (2006).
- [41] T. Plehn, D. Rainwater, and P. Skands, Phys. Lett. B **645**, 217 (2007).
- [42] J. Alwall, S. de Visscher, F. Maltoni, JHEP **0902** (2009) 017.
- [43] T. Sjöstrand, S. Mrenna and P. Z. Skands, JHEP **0605**, 026 (2006).
- [44] G. Bevilacqua, M. Czakon, C. G. Papadopoulos, R. Pittau, and M. Worek, JHEP **0909**, 109 (2009)
- [45] A. van Hameren, Comput. Phys. Commun. **182**, 2427 (2011).